Soraya GOUDER[1], Laatra YOUSFI[1], Dhaouadi GUIZA[1], Ramdane MAHAMDI[2], Isabelle BERBEZIER[3].

Echahid Cheikh Larbi Tebessi University, Algeria (1), University Mostefa Ben Boulaid-Batna 2, *Algeria* (2), Aix Marseille University, France (3)

doi:10.15199/48.2024.04.31

Optimizing SiGe-on-annealed DPSi Heterostructures Using Raman Spectroscopy and Genetic Algorithm for Enhanced Material Characterization and Performance

Abstract: *In our preceding investigation, we delved into the intricacies of SiGe alloys on double porous silicon (DPSi) through Raman spectroscopy, uncovering previously unknown connections between Raman peak shifts, stresses, and the concentration of Ge in the SiGe alloys in porous materials.A standout feature of this study lies in its distinct approach — a comparison of results employing a genetic algorithm. This method offers a comprehensive analysis of the data, enhancing our understanding of the intricate relationships at play. Validated through the frequency method, our results yield valuable insights into epitaxial growth on DPSi, presenting a nuanced perspective on the intricate interplay between Raman spectroscopy, stress, and alloy composition. These findings not only contribute to the evolving understanding of SiGe alloys but also pave the way for further advancements in the field of epitaxial growth on innovative substrates like DPSi*

Streszczenie. *W naszym poprzednim badaniu zagłębiliśmy się w zawiłości stopów SiGe na podwójnie porowatym krzemie (DPSi) za pomocą spektroskopii Ramana, odkrywając nieznane wcześniej powiązania między przesunięciami pików Ramana, naprężeniami i stężeniem Ge w stopach SiGe w materiałach porowatych. Cechą tego badania jest odrębność podejścia — porównanie wyników z wykorzystaniem algorytmu genetycznego. Metoda ta umożliwia wszechstronną analizę danych, co pozwala lepiej zrozumieć złożone zależności. Nasze wyniki, potwierdzone metodą częstotliwości, dostarczają cennych informacji na temat wzrostu epitaksjalnego na DPSi, prezentując zniuansowaną perspektywę na skomplikowane wzajemne oddziaływanie między spektroskopią Ramana, naprężeniem i składem stopu. Odkrycia te nie tylko przyczyniają się do lepszego zrozumienia stopów SiGe, ale także torują drogę do dalszych postępów w dziedzinie wzrostu epitaksjalnego na innowacyjnych podłożach, takich jak DPSi (**Optymalizacja heterostruktur DPSi wyżarzonych SiGe przy użyciu spektroskopii Ramana i algorytmu genetycznego w celu uzyskania lepszej charakterystyki i wydajności materiałów**)*

Keywords: Double porous Silicon, Raman spectroscopy, genetic algorithm.
Słowa kluczowe: Krzem podwójnie porowaty, spektroskopia ramanowska, algorytm genetyczny.

1. Introduction

Recent technological advancements have highlighted the importance of both reducing device dimensions and enhancing their performance. Consequently, there is a growing need to control stress in structures and understand its origin. An emerging and promising strategy involves employing compliant substrates, with porous silicon (PSi) standing out due to its recognized flexibility [1, 5]. The pliant and supple characteristics of PSi enable it to adeptly absorb the stress shift induced by SiGe heteroepitaxial films, primarily owing to its elevated pore density. Its harmonious fit with silicon-based microelectronics and its cost-effectiveness have unlocked fresh opportunities for incorporating diverse supra-axial systems (such as III-V or SiGe) onto silicon substrates [6, 7].

Recently, double porous Si (DPSi) has emerged as a prominent candidate in the competitive quest for compliant substrates, particularly for epitaxial growth in heterogeneous systems (such as III-V and SiGe) on Si [8]. The double porous silicon (DPSi) structure comprises an ultrathin, atomically flat upper layer with sealed pores and a thick, highly porous layer beneath. However, endeavors to achieve low-temperature epitaxy of SiGe and Ge on this DPSi layer led to the development of uneven epitaxial layers characterized by the presence of extended defects. [9, 10].

Nevertheless, subjecting the DPSi layer to thermal treatment induces substantial morphological alterations, transforming small pores into larger ones while concurrently producing tensile strain, as previously documented in our earlier research [1]. This pseudosubstrate possesses two remarkable properties: it is highly flexible and undergoes tensile strain which opens up possibilities for effectively integrating heterogeneous systems on Si by using annealed DPSi.

This study delves into the exploration of annealed DPSi as a stressor template layer to deposit a high-quality monocrystalline SiGe layers by molecular beam epitaxy (MBE). Then, our primary focus was on the analysis of the continuous variation trend of Ge content (x) and strain, aiming to quantitatively determine the distribution of Ge content (x) and strain.

In our previous work [11], we derived equations using the frequency method that describe the variation of Raman spectra with germanium (Ge) content and strain in SiGe alloys grown on DPSi. These equations, providing valuable insights into the complex interplay of composition and strain in SiGe, have significantly contributed to our understanding of these materials. Building upon these findings, the current study employs a different approach to validate the obtained parameters using a genetic algorithm.The combination of the frequency method and the genetic algorithm enhances the robustness and reliability of our results, offering a comprehensive analysis of the relationships between spectral features, composition, and strain in SiGe alloys.

Genetic algorithms stand as among the most extensively employed evolutionary techniques, prized for their strong performance and straightforward integration. However, the efficacy of these algorithms is predominantly contingent upon the selection of the appropriate search space [12]. The complete details of this calculation method are listed below in section 3.3.

By using these equations, valuable information about the composition and strain can be obtained for SiGe grown on annealed DPSi from Raman spectra.

The rest of this investigation is structured as follows: The second section is dedicated to the experimental examination, involving the preparation of samples using the MBE technique to attain SiGe on annealed DPSi structures. Moving to the third segment, we present the preliminary exploration of Raman spectroscopy in conjunction with a genetic algorithm ultimately, the study concludes with a summary at the culmination of this work.

2. Experimental

The growth experiments were conducted using MBE technique in a Riber system. To obtain DPSi structures, a (001)-oriented B-doped Si wafer was immersed in hydrofluoric acid (HF 25%) through electrochemical etching. By varying the current density between 10 mA.cm^{-2} and 80 mA.cm^{-2}, porosities ranging from 20% and 30% were achieved [8]. Prior to introducing the DPSi layers into the growth chamber, they underwent an annealing process under a hydrogen atmosphere at a high temperature (T) of 1100°C for 60 seconds. The annealing process facilitated the generation of a stable porous layer with improved structural and optical characteristics. To prepare the samples, we followed the identical cleaning procedure as previously outlined in our earlier work [1]. Subsequently, the samples were immediately introduced into an ultra-high vacuum chamber and subjected to outgassing at 400°C for 15min to prevent surface contamination. Above the SiGe layers, an ultrathin Si buffer layer was grown by MBE in ultrahigh vacuum (UHV) in order to avoid unintentional surface contamination. The deposition of SiGe layers took place at 500°C.

Raman measurements were conducted using a Bruker spectrophotometer (SENTERIA), with excitation achieved using a beam of 488 nm line from an argon laser operating at an output power of 10 mW.

3. Results and discussion

The characteristics of SiGe are significantly influenced by both its composition and stress. Stress has a notable impact on the energy band structure and lattice vibration, while composition affects the lattice constant and electron mobility [13, 14]. Raman spectroscopy proves to be a valuable tool for characterizing these factors, typically capturing the peaks of Si-Si, Si-Ge, and Ge-Ge modes in SiGe. As both composition and strain can induce shifts in the Raman peaks, a detailed analysis of the Raman spectra allows for the precise calculation of these values.

In the literature, numerous sets of equations establish connections between the frequencies of Si-Si, Ge-Ge and Si-Ge peaks with Ge content and strain, these equations are typically presented in the following format [15, 16]:

$$(1a)\quad \omega^{Si-Si} = \omega_0^{Si-Si} - A^{Si-Si}x + b^{Si-Si}\varepsilon_{/\!/}$$
$$(1b)\quad \omega^{Ge-Ge} = \omega_0^{Ge-Ge} - A^{Ge-Ge}x + b^{Ge-Ge}\varepsilon_{/\!/}$$
$$(1c)\quad \omega^{Si-Ge} = \omega_0^{Si-Ge} - A^{Si-Ge}x + b^{Si-Ge}\varepsilon_{/\!/}$$

Here, $A^{i-j}$and b^{i-j} represent the coefficients that relate the shift of Si-Si, Ge-Ge and Si-Ge vibrations to the Ge concentration and strain.

The values of mode frequencies extrapolated to x→0 are represented by ω_0^{i-j}.

In our prior research[11], we derived this set of equations elucidating the variation of Raman spectra concerning Ge content and strain in SiGe alloys grown on DPSi. The resulting relationships are as follows:

$$(2a)\quad \omega^{Si-Si} = \omega_0^{Si-Si} + 26x - 811.5\varepsilon_{/\!/}$$
$$(2b)\quad \omega^{Ge-Ge} = \omega_0^{Ge-Ge} + 54x - 373\varepsilon_{/\!/}$$
$$(2c)\quad \omega^{Si-Ge} = \omega_0^{Si-Ge} + 81x - 858.7\varepsilon_{/\!/}$$

We will now provide a revised description of the methodology employed to obtain these results.

3.1. Raman scattering

We have used the Raman spectra associated with SiGe substrates to accurately determine $A^{i-j}$and b^{i-j} the coefficients that link the shifts of Si–Si, Si–Ge, and Ge–Ge vibrations to the germanium concentration

Figure 1 displays the Raman spectra of various samples, each exhibiting three distinct peaks. The positions and energies of these peaks are influenced by both the Ge content (x) and the strain [17]. These peaks correspond to the optical phonons resulting from the motion of adjacent Si-Ge, Ge-Ge, and Si-Si pairs, as demonstrated in previous studies [17]. Furthermore, the positions of all three peaks shift relative to each other depending on the value of x. The three well-defined peaks are observed at approximately 514–518 cm^{-1} for Si-Si, 295–304 cm^{-1} for Ge-Ge, and 412–408 cm^{-1} for Si-Ge.

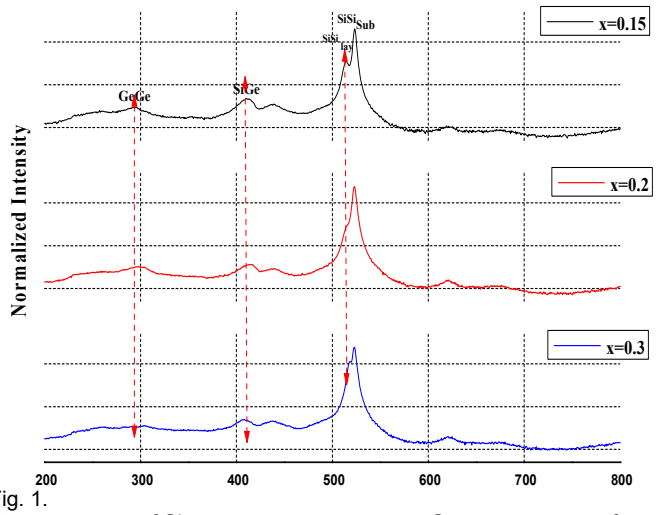

Fig. 1. Raman spectra of Si$_{1-x}$Ge$_x$ grown on top of annealed DPSi [11].

It is evident that the Raman Ge-Ge peak undergoes a shift towards lower frequencies (or higher frequencies for x=0.3) relative to Ge-Ge mode observed in Ge bulk (at 300 cm^{-1}), which is assigned to both composition and strain influences. Additionally, the Si-Ge modes show peak intensities above 408 cm^{-1}, which contrasts with the growth of SiGe on a monolayer system where the corresponding mode was seen at lower frequencies (393 cm^{-1}), as demonstrated in a previous work [18].

The observed results can be attributed to the inherent microstructure characteristics of annealed DPSi. Specifically, the heating process leads to the development of tensile strain within DPSi due to the release of volatile species that were incorporated into PSi during the electrochemical fabrication process. Figure 2 further illustrates these structural changes, presenting the Raman spectrum of annealed DPSi alongside the Raman spectra of the as-etched PSi. The Raman peak of DPSi undergoes a higher wavenumber shift to 523 cm^{-1}, corresponding to the relaxation of lattice expansion and the restructuring of porous morphology induced by annealing [19]. This modification is linked to an increase in pore diameter, a phenomenon previously demonstrated in our earlier research [1]. However, the Raman spectrum peak of PSi is observed at a slightly different shift, specifically 520 cm^{-1} (notably, the Raman peak of the monocrystalline Si wafer is situated at 521 cm^{-1}). This shift in peak position is attributed to tensile stress in the porous film caused by lattice expansion during anode etching. The phonon confinement mode, considering the effects of mechanical stresses, can elucidate this phenomenon.

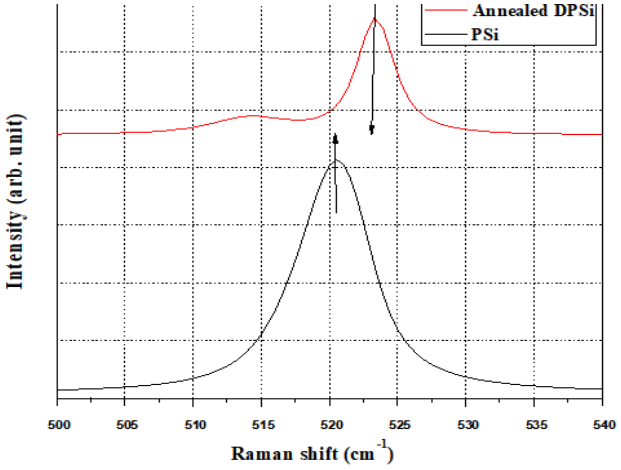

Fig. 2. The Raman spectra of annealed DPSi, And as-etched PSi [11].

The presence of an additional Raman peak at 514 cm⁻¹ suggests the presence of a tensile-strained layer within the thin, pore-free PSi layer. The tensile strain observed in DPSi is a consequence of elevated-temperature annealing, which prompts an expansion of the lattice structure. This expansion is instigated by the elimination of hydrogen during thermal annealing, resulting in a notable reduction in the lattice parameter.

3.2. Equations for SiGe on annealed DPSi

The approach employed entails using a series of experimental equations derived from the peak positions of the Si-Si, Si-Ge, and Ge-Ge modes. The relationships between phonon frequencies and the Ge content (x), as obtained in our prior work [11], are outlined below:

$$(3a) \quad \omega^{Si-Si} = 511 + 26.5x$$

$$(3b) \quad \omega^{Ge-Ge} = 286.5 + 59x$$

$$(3c) \quad \omega^{Si-Ge} = 366.7 + 466x - 109.5x^2$$

The Si-Si (Ge-Ge) peak frequency exhibits a linear increase with rising Ge content, while the Si-Ge mode demonstrates a nonlinear behavior. These equations enable us to determine the ω_0^{i-j} values. Subsequently, these values are substituted into equations (1) with the Raman peak positions to obtain $A^{i-j}$and b^{i-j}. While the values of A^{i-j} can be calculated straightforwardly, computing the coefficients b^{i-j} is a more intricate process. This complexity arises from their connection between deformation and changes in Raman frequency. To calculate these coefficients, we employed the equation referenced in [20, 21].

$$(4) \quad b^{i-j} = \frac{1}{2\omega_0}\left(-\frac{2C_{12}}{C_{11}}p + 2q\right)$$

After completing the detailed calculations outlined in our article [ref], we derived the following values: $A^{Si-Si} = -26$, $A^{Ge-Ge} = -54$ and $A^{Si-Ge} = -81$ for the coefficients A^{i-j}. Additionaly, $b^{Si-Si} = -811.5$ cm^{-1}, $b^{Ge-Ge} = -373$cm^{-1} and $b^{Si-Ge} = -858.72$ for the coefficients b^{i-j}, which leads to a set of equations mentioned above:

$$(5a) \quad \omega^{Si-Si} = \omega_0^{Si-Si} + 26x - 811.5\varepsilon_{//}$$

$$(5b) \quad \omega^{Ge-Ge} = \omega_0^{Ge-Ge} + 54x - 373\varepsilon_{//}$$

$$(5c) \quad \omega^{Si-Ge} = \omega_0^{Si-Ge} + 81x - 858.7\varepsilon_{//}$$

Considering the set of equations obtained by measuring the experimental position of the three phonon lines ω^{i-j}, a combination of any pair of the three equations allows for the determination Ge content (x) and strain (ε) in the SiGe layer.

To be confident that the results obtained demonstrate the effectiveness of Raman spectroscopy in determining Ge content (x) and evaluating strain or relaxation levels in the monocrystalline SiGe grown on annealed DPSi, an alternative approach has been employed to provide the set of equation that link frequencies of Si-Si, Ge-Ge and Si-Ge peaks with Ge content and strain. A genetic algorithm has been utilized for this purpose.

3.3. Enhancing SiGe-on-annealed-DPSi equation using Genetic Algorithm

Genetic algorithms are the most widely used evolutionary methods known for their robust performance and seamless integration. These algorithms differ from conventional search and optimization techniques due to their focus on manipulating parameter encodings rather than the parameters directly. They are inherently designed for maximization, setting them apart. These distinctions allow genetic algorithms to find global optimal points, rendering them highly suitable for addressing a large variety of problems [22].

Nonetheless, the effectiveness of these algorithms largely relies on choosing the appropriate search space. From the set of equations 1, we have to determine the coefficients A^{i-j}, $b^{i-j}$and the strain ε. the ω^{i-j} symbols represent the Raman wavenumbers obtained from the experiments, while the ω_0^{i-j} symbols correspond to the mode frequencies extrapolated to the limit as x approaches 0. Hence, the process of parameter identification involves finding the vector X= [A^{i-j} b^{i-j} ω_0^{i-j}] by minimisation of Root Mean Square Error (RMSE) between the experimental values of ω_e^{i-j} from Raman spectroscopy and the calculated ones ω_c^{i-j} from genetic algorithm which is represented by the equation:

$$(6) \quad RMSE = \sqrt{\frac{1}{n}\sum_n\left(\omega_e^{i-j} - \omega_c^{i-j}\right)^2}$$

The fundamentals of the basic genetic algorithm are straightforward, encompassing tasks as uncomplicated as copying strings and swapping partial strings. The process commences with a randomly generated initial population of individuals. Subsequently, this population undergoes iterative evolution via a string manipulation mechanism employing three genetic operators: selection (reproduction), crossover, and mutation [22]. From data selection, Raman spectra are provided from a series of SiGe alloy samples with varying compositions. Each spectrum corresponds to a different SiGe alloy composition. Then, the genetic algorithm process involves the following steps [23]:

Step 1 (Chromosome representation): each chromosome encodes a particular SiGe alloy composition, with genes representing the desired parameters.

Chromosome$_l$= [X_1……X_n] where X_{min}<$X_{1,\ldots,n}$<X_{max} and l=1, 2,…, N_p

Each vector X contains the variables that are mentioned above. We have to highlight the role of Raman spectroscopy in guiding the algorithm toward values of parameters by providing it with desirable compositions and experimental Raman wavenumbers.

Step 2 (Fitness function): Compute the fitness function value for every chromosome, based on the Raman spectra and the alloy composition.
Step 3 (Selection and crossover): The genetic algorithm selects parent parameters based on fitness values and performs crossover to generate new values of parameters with exchanging the subsequences between the two parents. It Utilize the operators outlined below:

a. Conduct reproduction by choosing optimal chromosomes probabilistically according to their fitness function values.
b. Execute crossover on the chromosomes chosen in the previous step using the specified crossover probability.
c. Carry out mutation on the chromosomes produced in the preceding step using the designated mutation probability.

The genetic algorithm is run for multiple generations, allowing it to evolve the values of parameters. At each iteration, the algorithm generates new values on the parent ones, guided by the fitness function and Raman spectroscopy, as resumed in step 4 and step 5:
Step 4: When the stopping condition is met or the optimal solution is attained, the procedure can be halted. Otherwise, iterate through Steps 2 to 4 until the stopping condition is satisfied.
Step 5: Obtain the optimal solution X^* that corresponds to the best value of the fitness function.
It's important to keep in mind that the desired parameters are A^{i-j} and b^{i-j} within the framework of set of equation 2, where *i* and *j* represent either Si or Ge.
The computation is performed separately for each of the three modes. The resultant estimated parameters values for Si-Si and Ge-Ge modes are shown in table 1.

Table 1. Parameters estimation of Si-Si and Ge-Ge modes using Genetic algorithm

	Vector of parameters X= [A^{i-j} b^{i-j} ω_0^{i-j}]	Fitness function
Si-Si	[26.0000 -823.1489 519.2056]	5.6730e-009
Ge-Ge	[-59.0000 -379.3014 294.9701]	0.1080

Figures 3 and 4 show the current best individual with the different corresponding parameter values. Additionally, they show the best fitness plotted versus generations for both Si-Si and Ge-Ge simultaneously.

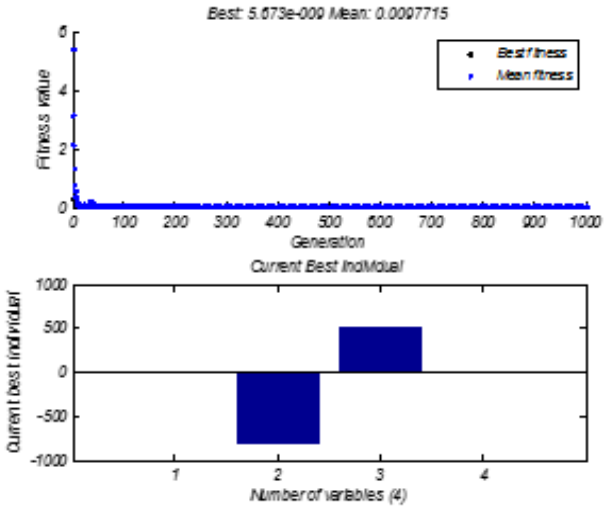

Fig. 3. Best Fitness and best individual for Si-Si

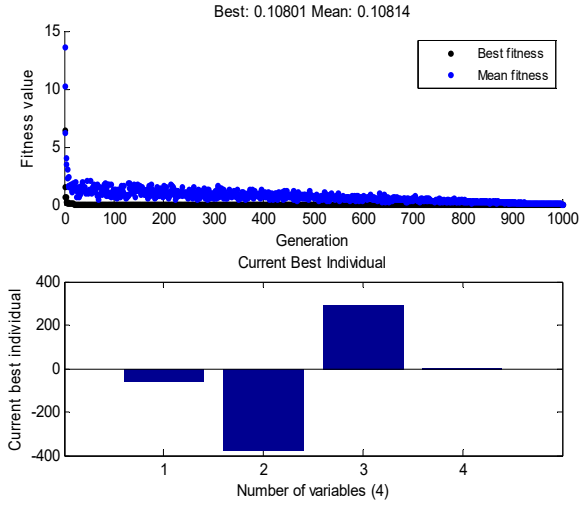

Fig. 4. Best Fitness and best individual for Ge-Ge.

The best optimal fitness value of the Si-Ge mode is given for a global optimal points, it illustrated in Figure 5, yielding the subsequent result: X= [-81.7182 -851.5134 400.9985].

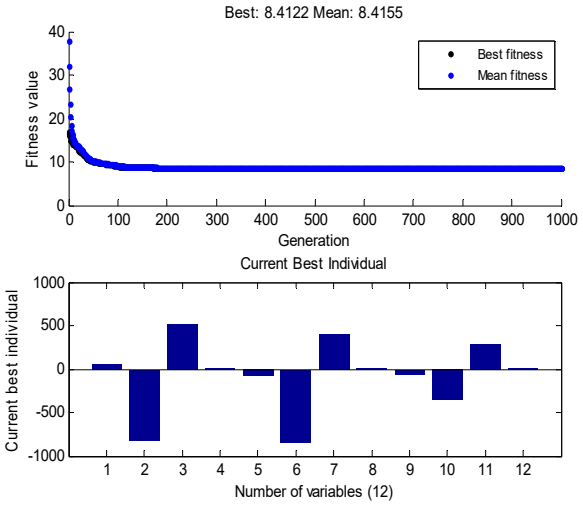

Fig. 5. Best Fitness and best individual for all modes

It's important to highlight that the strain values acquired do not go beyond 0.015 for any of the samples. Furthermore, the obtained reference peak positions ω_0^{i-j} for various modes when x is near 0: $\omega_0^{Si-Si} = 519.2056\text{cm}^{-1}$, $\omega_0^{Ge-Ge} = 294.9701\ \text{cm}^{-1}$ and ω_0^{Si-Ge}=400.9985 cm^{-1} exhibit a closer resemblance to the values documented in literature [17, 24] compared to those derived through the frequency method.
The set of equation obtained is written as follows:

$$(7a) \quad \omega^{Si-Si} = \omega_0^{Si-Si} - 26x - 823\varepsilon_{//}$$

$$(7b) \quad \omega^{Ge-Ge} = \omega_0^{Ge-Ge} + 59x - 379\varepsilon_{//}$$

$$(7c) \quad \omega^{Si-Ge} = \omega_0^{Si-Ge} + 82x - 852\varepsilon_{//}$$

The computation of the coefficients (A^{i-j} and b^{i-j}) boast a high level of precision, with error bars generally amounting to 0.1% and lower. Inaccuracies in Raman measurements primarily stem from slight deviations related to the peak positions of ω^{Si-Si}, ω^{Ge-Ge} and ω^{Si-Ge}, the interdependence of ω^{Si-Si} , ω^{Ge-Ge} and ω^{Si-Ge} concerning x and $\varepsilon_{//}$ has been ascertained with noteworthy accuracy. The

disparity in outcomes between the frequency method using Raman spectroscopy and the genetic algorithm lies in terms of strain (denoted b^{i-j}). Numerous research efforts have been dedicated to investigating the identification of potential distortions in optical phonons within SiGe, with a particular focus on the b^{i-j} coefficients that establish the connection between Raman frequency shifts and deformations. Although the calculation of A^{i-j} has been achieved with relatively high accuracy (usually resulting in zero difference bars), There is a slight disparity between the values of b^{i-j} obtained through the genetic algorithm and the frequency method. The stress tensor remains independent of the variable x, yet it is correlated with ε through the parameters of b^{i-j}. The annealed DPSi material can accommodate substantial strain by virtue of its combined tensile strain and soft behaviour. The strain induced by the tensile layer can modify the properties of the grown SiGe.

By utilizing the frequencies of the three modes, we were able to concurrently derive both the composition and the in-plane strain within a predefined concentration range efficiently. Depending on the concentration of Ge, it is recommended to employ these correlations particularly for lower Ge contents (≤ 0.35), aiming to reduce potential uncertainties.

4. Conclusion

In summary, we have introduced the initial direct exploration of Raman spectroscopy along with a genetic algorithm for formulating a set of equations that establish a connection between phonon frequencies and the Ge content (x) as well as strain ($\varepsilon_{//}$). The A^{i-j} values exhibit near equivalence between the two methods, whereas a marginal 1% discrepancy is observed for the b^{i-j} parameters across all modes. Nonetheless, this discrepancy does not negate the assertion that the genetic algorithm method is more precise and offers a quicker solution.

Raman spectroscopy and a genetic algorithm can be applied to optimize SiGe alloy compositions for microelectronics applications. The integration of Raman spectroscopy data with an optimization algorithm can lead to improved semiconductor device performance and contribute to advancements in the microelectronics field.

Acknowledgments

The authors would like to express their gratitude to the STM laboratory for providing the PSi samples.

***Authors**: Ph.D. Soraya GOUDER, email: soraya.gouder@univ-tebessa.dz, Ph.D. Laatra YOUSFI, email: laatra.yousfi@univ-tebessa.dz. Ph. D. Dhaouadi GUIZA, email:dhaouadi.guiza@univ-tebessa.dz, Department of Electrical Engineering, Faculty of Sciences and Technology,Echahid Cheikh Larbi Tebessi university, Tebessa, Algeria,Prof. Ramdane MAHAMDI, email: r.mahamdi@univ-batna2.dz, LEA, department of Electronics, University Mostefa Ben Boulaid-Batna 2, Batna 05000, Algeria, Prof. Isabelle BERBEZIER, email: isabelle.berbezier@im2np.fr, Aix Marseille University IM2NP, 142 Avenue. Escadrille Normandie Niemen, 13013 Marseille, France.*

REFERENCES

[1] *Gouder, S., Mahamdi, R., Aouassa, M., Escoubas, S., Favre, L., Ronda, A., and Berbezier, I.: Investigation of microstructure and morphology for the Ge on Porous Silicon/Si substrate hetero-structure obtained by Molecular Beam Epitaxy, Thin Solid Films, 550, pp. 233- 238, Jan. 2014.*

[2] *Aouassa, M., Escoubas, S., Ronda, A., Favre, L., Gouder, S., Mahamdi, R., Arbaoui, E., Halimaoui, A., and Berbezier, I.: Ultra-thin planar fully relaxed Ge pseudo-substrate on compliant porous silicon template layer, Applied. Physics. Letters. 101(23), pp. 233105, Dec. 2012.*

[3] *Huang, M., Ritz, C. S., Novakovic, B., Yu, D., Zhang, Y., Flack, F., Savage, D. E., Evans, P. G., Knezevic, I., Liu, F., and Lagally, M. G.: Mechano-electronic Superlattices in Silicon Nanoribbons, ACS Nano. 3 (3), pp. 721-727, Feb. 2009.*

[4] *Malachias, A., Mei, Y., Annabattula, R. K., Deneke, C., Onck, P. R., and Schmidt, O. G.: Wrinkled-up Nanochannel Networks: Long-Range Ordering, Scalability, and X-ray Investigation, ACS Nano. 2(8), pp. 1715-1721, Jul. 2008.*

[5] *Khang, D. –Y., Jiang, H., Huang, Y., and Rogers, J. A.: A stretchable form of single-crystal silicon for high-performance electronics on rubber substrates, Science, 311 (5758), pp. 208-212, Feb. 2006.*

[6] *Seungwan, W., Geunhwan, R., Taesoo, K., Namgi, H., Jae-Hoon, H., Rafael Jumar, C., Jinho, B., Jihyun, K., In-Hwan, L., Deahwan, J., and Won Jun, C.: Growth and Fabrication of GaAs Thin-Film Solar Cells on a Si Substrate via Hetero Epitaxial Lift-Off, Applied. Sciences. 2022, 12 (2), pp. 820, Jan. 2022https://doi.org/10.3390/app12020820*

[7] *Sang Hyeon, K., Min-Su, P., Dae-Myeong, G., Hosung, K., GuenHwan, R., Hyunduk, Y., Jindong, S., Chagzoo, K., and Won Jun, C.: Fabrication and Characterization of Single junction GaAs solar cell epitaxially grown on Si substrate, Current Applied Physics 15; DOI: 10.1016/j.cap.2015.04.022, Current Applied Physics, 15 (2), pp. S40-S43, Sep. 2015, https://doi.org/10.1016/j.cap.2015.04.022*

[8] *Berbezier, I., Aqua, J. N., Aouassa, M., Favre, L., Escoubas, S., Gouye, A., and Ronda, A. : Accomodation of SiGe strain on a universally compliant porous silicon substrate, Physical Review B, 90 (3), pp. 035315-035320, Jul. 2014.*

[9] *Gardelis, S., Nassiopoulou, A. G., Mahdouani, M., Bourguiga, R., and Jaziri, S. : Enhancement and red shift of photoluminescence (PL) of fresh porous Si under prolonged laser irradiation or ageing: Role of surface vibration modes, Physica E: Low-dimensional Systems and Nanostructures, 41 (6), pp. 986-989, May. 2009.*

[10] *Hariharsudan, S. R., Roberto, M., Depauw, V., Nieuwenhuysen, K. V., Bearda. T., Gordon, I., Szlufcik, J., and PoortmansKerfless, J.: layer-transfer of thin epitaxial silicon foils using novel multiple layer porous silicon stacks with near 100% detachment yield and large minority carrier diffusion lengths; Solar Energy Materials and Solar Cells 135, pp. 113-123, Apr. 2015. https://doi.org/10.1016/j.solmat.2014.10.049*

[11] *Gouder, S., Mahamdi, R., Guiza, D., Berbezier, I. (2023). Vibrational properties and raman peak shift relationships in Si1−xGex epilayers grown on annealed double porous silicon. Revue des Composites et des Matériaux Avancés-Journal of Composite and Advanced Materials, 33(5), pp. 275-281. Oct. 2023. https://doi.org/10.18280/rcma.330501*

[12] *Yong. Z., and Sannomiga, N.: An improvement of genetic algorithms by search space reduction solving large-scale flow shop problems, IEE Japan Transactions on Electronics Information and Systems, 121 (6), pp. 1010-1015, Jun. 2001.*

[13] *Jian-Jun, S., He-Ming, Z., Hui-Yong, H., Xian-Ying, D., and Rong-Xi, X.: Determination of conduction band edge characteristics of strained Si/Si1-xGex, Chinese Physics, 16(12), pp. 3827-3831, Dec. 2007.*

[14] *Fu, Y., and Willander, M.: Hole conduction characteristics of strained Si1−xGex/Si resonant tunnelling diode; Physica E: Low-dimensional Systems and Nanostructures, pp. 72-79, Feb. 2002, https://doi.org/10.1016/S1386-9477(01)00228-4;*

[15] *Rouchon, D., Mermoux , M., Bertin, F., and Hartmann , J. M.: Germanium content and strain in Si1-xGex alloys characterized by Raman spectroscopy. Journal of Crystal Growth, 392, pp. 66-73, Apr. 2014.*

[16] *Wong, L. H., Wong, C. C., Liu, J. P., sohn, D. K., Chan. L., Hsia, L. C., Zang, H., Ni, Z. H., and Shen, Z. X.: Determination of Raman Phonon Strain Shift Coefficient of Strained Silicon and Strained SiGe. Japanese Journal of Applied Physics, 44(11), pp. 7922–7924, Nov. 2005.*

[17] *Perova, T. S., Wasyluk, J., Lyutovich, K., Kasper, E., Oehme, M., Rode, K., and Waldron, A.: Composition and strain in thin*

Si1-xGex virtual substrates measured by microRaman spectroscopy and X-ray diffraction. Journal of applied physics, 109 (3), pp. 033502. Feb. 2011

[18] *Aouassa, M., Jadli, I., Slimen Hassayoun, L., Maaref, H., Panczer, G., Favre, L., Ronda, A., Berbezier, I.: Analysis of composition and microstructures of Ge grown on porous silicon using Raman spectroscopy and Transmission Electron Microscopy. Superlattices and Microstructures. 112: pp. 493-498. Dec. 2017. https://doi.org/10.1016/j.spmi.2017.10.003.*

[19] *Karim, ?K., Martini, R., Radhakrishnan, H. S.,Nieuwenhuysen, K. V., Depauw, V., Wedgan, R., Gordon, I., and Jef Poortmans.: Tuning of strain and surface roughness of porous silicon layers for higher-quality seeds for epitaxial growth; Nanoscale Research Letters, 9:348, Jul. 2014. http://www.nanoscalereslett.com/content/9/1/348*

[20] *Rouchon, D., Mermoux , M., Bertin, F., and Hartmann , J. M.: Germanium content and strain in Si1-xGex alloys characterized by Raman spectroscopy. Journal of Crystal Growth, 392, pp. 66-73, Apr. 2014.*

[21] *Wong, L. H., Wong, C. C., Liu, J. P., sohn, D. K., Chan. L., Hsia, L. C., Zang, H., Ni, Z. H., and Shen, Z. X.: Determination of Raman Phonon Strain Shift Coefficient of Strained Silicon and Strained SiGe. Japanese Journal of Applied Physics, 44(11), pp. 7922–7924, Nov. 2005.*

[22] *Emara, H. M., Elshamy, W., and Bahgat, A.: Parameter Identification of Induction Motor Using Modified Particle Swarm Optimization Algorithm, IEEE International Sympsium on Industrial Electronics (ISIE), Cairo University, Jun. 2008*

[23] *Yousfi, L., Bouchemha, A., Bechouat, M., and Boukrouche, A.: Vector control of induction machine using PI controller optimized by genetic algorithms. 16th International Power Electronics and Motion Control Conference and Exposition, Antalya, Turkey 21-24 Sept 2014*

[24] *Tsang, J. C., Mooney, P. M., Dacol, F., and Chu, J. O.: Measurements of alloy composition and strain in thin GexSi1-xlayers, Journal of Applied Physics, 75(12), pp. 8098, 1994.*